The Astrophysical Journal Supplement Series, 194:33 (6pp), 2011 June doi:10.1088/0067-0049/194/2/33

IMPLEMENTATION OF THE GRADUATED CYLINDRICAL SHELL MODEL FOR THE THREE-DIMENSIONAL RECONSTRUCTION OF CORONAL MASS EJECTIONS

A. Thernisien
ARTEP Inc., Ellicott City, MD 21042, USA
Received 2011 February 7; accepted 2011 March 31; published 2011 May 26

ABSTRACT

The graduated cylindrical shell (GCS) model developed by Thernisien et al. has been used with the goal of studying the three-dimensional morphology, position, and kinematics of coronal mass ejections observed by coronagraphs. These studies focused more on the results rather than the details of the model itself. As more researchers begin to use the model, it becomes necessary to provide a deeper discussion on how it is derived, which is the purpose of this paper. The model is built using the following features and constraints: (1) the legs are conical, (2) the front is pseudo-circular, (3) the cross section is circular, and (4) it expands in a self-similar way. We derive the equation of the model from these constraints. We also show that the ice-cream cone model is a limit of the GCS when the two legs overlap completely. Finally, we provide formulae for the calculation of various geometrical dimensions, such as angular width and aspect ratio, as well as the pseudo-code that is used for its computer implementation.

Key words: methods: data analysis – methods: numerical – Sun: coronal mass ejections

1. INTRODUCTION

The graduated cylindrical shell (GCS) is an empirical model to represent the flux rope structure of some coronal mass ejections (CMEs). CMEs are expulsions of plasma in the solar corona which are regularly recorded by white-light coronagraphs such as the Large Angle and Spectromeric Coronagraph Experiment (LASCO; Brueckner et al. 1995) on board the *Solar and Heliospheric Observatory* (*SOHO*) mission (Domingo et al. 1995), and SECCHI (Howard et al. 2008) on board the *STEREO* mission (Kaiser et al. 2008). After decades of CME observations and classification based on their morphological similarities (e.g., Howard et al. 1985), the flux rope morphology is emerging as the most typical three-dimensional shape we can use to represent CMEs. For example, Chen et al. (1997) used an idealized flux rope model to successfully reproduce the main features of a CME observed with LASCO.

Another important property of CMEs is that they tend to expand self-similarly (Chen et al. 1997, 2000; Cremades & Bothmer 2004; Chen et al. 2006). The GCS model is developed to integrate both the self-similar expansion and the flux rope three-dimensional morphology. Thernisien et al. (2006) used it to fit a sample of 34 CMEs observed with LASCO and 26 CMEs observed with *STEREO–SECCHI* (Thernisien et al. 2009). They showed that coronagraph observations of CMEs, even from different viewpoints, could be reproduced to the first order with this type of morphology. They also showed that the model can be used to obtain estimations of parameters such as CME position, direction, three-dimensional extent, true speed, and even, but with a smaller confidence, its orientation (see Thernisien et al. 2009; Liu et al. 2010).

Since its introduction, the GCS has been employed in many other studies. For example, Poomvises et al. (2010) determined the kinematics and expansion speed of four events from 5 $R_\odot$ to 80 $R_\odot$ using the *STEREO*/*SECCHI* COR2 and Heliospheric Imager instrument fields of view. Lynch et al. (2010) used it to determine the flux rope orientation and rotation in coronagraph images and then compared the results to flux rope fitting using in situ data. Liu et al. (2010) compared the GCS modeling of two CME events with flux rope reconstruction using in situ measurements at 1 AU. Finally, Patsourakos et al. (2010) used it on *SECCHI* EUVI images to study the three-dimensional evolution and expansion of a cavity that later lead to a CME event and the formation of a post-CME current sheet from multiviewpoint observations (Patsourakos & Vourlidas 2011).

Our two original studies (Thernisien et al. 2006, 2009) restricted much of the discussion to scientific results, giving little space to the details of the model construction and implementation. As more researchers begin to use the model, it becomes necessary to provide a deeper discussion of its derivation, which is the purpose of this paper. The goal is to give a reference for any author that has used or plans to use the model.

2. DERIVATION OF THE MODEL

2.1. Description of the Model

The GCS is often called the "hollow croissant" because of its shape. Figure 1 gives the schematic of the model: the left panel shows a planar cut of the croissant viewed face-on, while the right panel shows a planar cut of the same croissant viewed edge-on. The electron density is placed only on the outer shell (or skin) of the croissant and the inside of the structure is hollow. The two legs are conical and the front is reminiscent of a torus with its cross-section radius increasing with height. We use an orthonormal and direct coordinate system noted $(O, \boldsymbol{x}, \boldsymbol{y}, \boldsymbol{z})$. The origin O is in the plane of both views. In practice, O corresponds to the center of the Sun. Note that the planes $(O, \boldsymbol{x}, \boldsymbol{y})$ and $(O, \boldsymbol{y}, \boldsymbol{z})$ are both planes of symmetry, and $(O, \boldsymbol{y})$ is an axis of symmetry. Figure 2 shows a white-light rendering of the model using Thomson scattering (Billings 1966). The left and right panels present the same face-on and edge-on views as in Figure 1.

2.2. Derivation of the Model

The model consists in two shapes: the conical legs and the curved front. The derivation of the conical legs is straightforward since it is a well-known geometrical shape. The derivation of the curved front is a little more elaborated, but still consists in using simple constraints and basic geometry. Hereafter, we describe

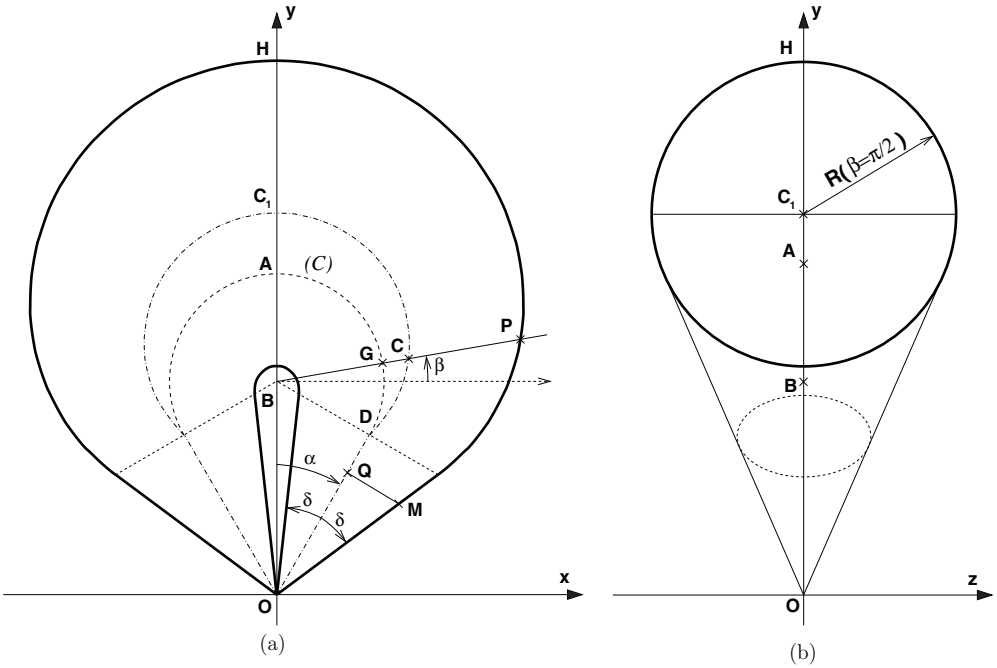

Figure 1. Schematic of the GCS model. The left panel shows a $(O, \boldsymbol{x}, \boldsymbol{y})$ planar cut of the croissant viewed face-on. The z-axis points toward the reader. The right panel shows a cut in the $(O, \boldsymbol{y}, \boldsymbol{z})$ plane where the croissant is viewed edge-on. In this view, only the circle (solid line) is in the $(O, \boldsymbol{y}, \boldsymbol{z})$ plane.

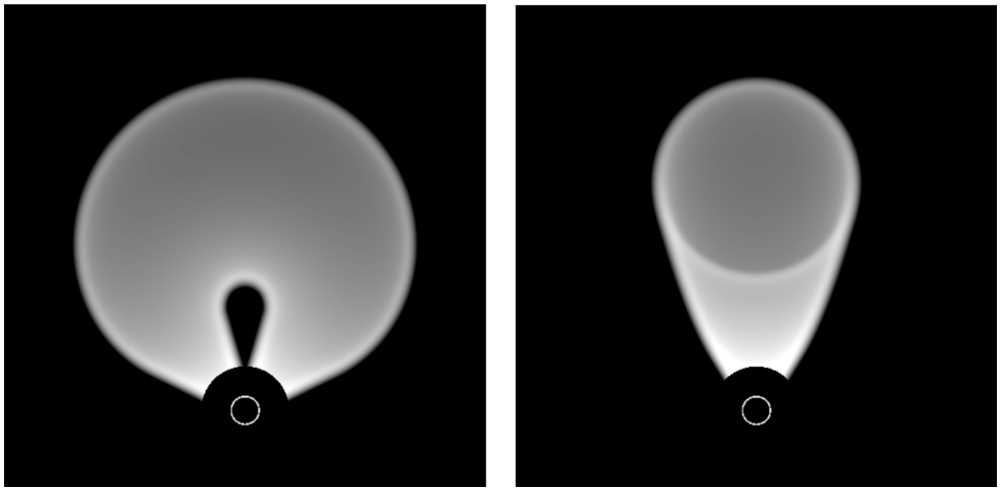

Figure 2. Rendered white-light images of the GCS model obtained by line-of-sight integration and using Thomson scattering (Billings 1966). The model orientations are the same as in Figure 1. Left: GCS model seen face-on. Right: GCS model seen edge-on.

the parameters of the model, then we define the constraints upon which the model is built. We follow with the calculation of the different parameters that permit us to construct the model.

We note (OD) the axis of the right leg as shown in Figure 1(a). The apex of the cone is at the origin O. The half-angle of the cone is noted δ, but we will use its sine κ:

$$\kappa = \sin\delta. \tag{1}$$

We call κ the aspect ratio of the model, as in Thernisien et al. (2006, 2009). This parameter sets the rate of expansion versus the height of the CME, so the structure expands in a self-similar way. The second parameter is the full height of the cone, which is the distance OD:

$$OD = h. \tag{2}$$

The third and last parameter, α, is the angle between the axis of the leg and the y-axis. α is called the half-angle. The three parameters κ, h, and α suffice to fully define the geometry of the model.

By definition, the cross section of the conical legs is circular. Let Q be a point on the leg axis and M a point on the cone so that $\overrightarrow{QM}$ is a radius of the cross section of the cone at the height $\overrightarrow{OQ}$. This way, we can write

$$\|\overrightarrow{QM}\| = \kappa\|\overrightarrow{OM}\|, \tag{3}$$

which is the self-similarity equation for the legs.

The front, and curved part of the model, is reminiscent of a torus with its cross-section radius varying with height. BC could be compared to the major radius of the torus, and R would

be the minor radius. The definition of the front is based on the following set of four constraints.

1. The circle ($\mathcal{C}$) with center B and radius BD, in the plane (O, $\boldsymbol{x}$, $\boldsymbol{y}$), is used as the generating line.
2. The points on the shell should follow the self-similarity equation.
3. The cross section of the shell is circular in the planes (B, $\overrightarrow{BG}$, $\boldsymbol{z}$), with G a point on ($\mathcal{C}$).
4. The center of the shell cross section is in the (O, $\boldsymbol{x}$, $\boldsymbol{y}$) plane.

These constraints not only define the shape of the front, but also ensure first-order continuity at the junction with the legs.

The first constraint is set with the circle ($\mathcal{C}$) of radius $\rho = BD$ and center B in the plane (O, $\boldsymbol{x}$, $\boldsymbol{z}$). B is the intersection between the plane containing the conical base, centered on D, and the $\boldsymbol{y}$-axis. The coordinates of B are $(0, b, 0)$, with

$$b = h/\cos\alpha. \tag{4}$$

If G is a point on ($\mathcal{C}$), the vector $\overrightarrow{BG}$ can be written as

$$\overrightarrow{BG} = \begin{pmatrix} \rho\cos\beta \\ \rho\sin\beta \\ 0 \end{pmatrix}, \tag{5}$$

where β is the angle between the $\boldsymbol{x}$-axis and $\overrightarrow{BG}$, and with

$$\rho = h\tan\alpha. \tag{6}$$

The self-similarity constraint for the front part can be written as

$$\|\overrightarrow{GP}\| = \kappa\|\overrightarrow{OP}\|, \tag{7}$$

where P is a point of the shell having for coordinates (x, y, z). Note that in Figure 1, P is plotted in the (O, $\boldsymbol{x}$, $\boldsymbol{y}$) plane, but in reality, it is not bound to be in that plane: the coordinate z does not have to be zero.

In order to express these constraints in terms of the model parameters, we write the vector $\overrightarrow{GP}$ as $\overrightarrow{GP} = \overrightarrow{GB} + \overrightarrow{BO} + \overrightarrow{OP}$, so that its vector components are

$$\overrightarrow{GP} = \begin{pmatrix} -\rho\cos\beta + x \\ -\rho\sin\beta - b + y \\ z \end{pmatrix}. \tag{8}$$

We can take the square of Equation (7) without changing the equality:

$$GP^2 = \kappa^2 OP^2. \tag{9}$$

By rewriting this equation in terms of the vector coordinates, we end up with the following equation:

$$\begin{aligned}(x^2 + y^2 + z^2)(1-\kappa^2) - 2x\rho\cos\beta - 2y(\rho\sin\beta + b) \\ + \rho^2 + b^2 + 2\rho b\sin\beta = 0.\end{aligned} \tag{10}$$

Finally, the last two constraints consist of forcing the equation of the shell to have the form of the equation of a circle in the (B, $\overrightarrow{BG}$, $\boldsymbol{z}$) plane and having its center, C, in the (O, $\boldsymbol{x}$, $\boldsymbol{y}$) plane. Toward this goal, we rewrite Equation (10) in the coordinate system (C, $\boldsymbol{X'}$, $\boldsymbol{Y}$, $\boldsymbol{z}$), using the following coordinate transforms.

1. Translation of the origin from O to B. The coordinate y can be expressed as a function of the new coordinate y':

$$y = y' + b, \tag{11}$$

so that Equation (10) can be rewritten as

$$\begin{aligned}(x^2 + y'^2 + z^2)(1-\kappa^2) - 2x\rho\cos\beta - 2y'(\rho\sin\beta + b\kappa^2) \\ + \rho^2 - b^2\kappa^2 = 0.\end{aligned} \tag{12}$$

2. Rotation around the axis (B, $\boldsymbol{z}$) by an angle β, so that the new $\boldsymbol{X}$-axis is aligned with $\overrightarrow{BG}$:

$$\begin{cases} x = X\cos\beta - Y\sin\beta \\ y' = X\sin\beta + Y\cos\beta \end{cases}, \tag{13}$$

so Equation (12) becomes

$$\begin{aligned}(X^2 + Y^2 + z^2)(1-\kappa^2) - 2X(\rho + b\kappa^2\sin\beta) \\ - 2Yb\kappa^2\cos\beta + \rho^2 - b^2\kappa^2 = 0.\end{aligned} \tag{14}$$

3. Translation from B to C:

$$X' = X + X_0, \tag{15}$$

so finally Equation (14) becomes

$$\begin{aligned}(X'^2 + Y^2 + z^2)(1-\kappa^2) - 2X'(\rho + b\kappa^2\sin\beta - X_0(1-\kappa^2)) \\ - 2Yb\kappa^2\cos\beta + X_0^2(1-\kappa^2) - 2X_0(\rho + b\kappa^2\sin\beta) \\ - b^2\kappa^2 + \rho^2 = 0.\end{aligned} \tag{16}$$

In order for the circular cross section to have its center at C and to be in the (C, $\boldsymbol{X'}$, $\boldsymbol{z}$) plane ($Y = 0$), Equation (16) should have the form of the equation of a circle centered at the origin of the coordinate system. This equation has the simple following form:

$$X'^2 + z^2 = R^2, \tag{17}$$

where R is the radius of the circle. If we identify the terms of Equations (16) and (17), we see that X_0 must be expressed as

$$X_0 = \frac{\rho + b\kappa^2\sin\beta}{1-\kappa^2}. \tag{18}$$

After some more, but still basic algebra, we can express R^2 as a function of X_0 and known parameters:

$$\begin{aligned} R^2 &= \frac{-X_0^2(1-\kappa^2) + 2X_0(\rho + b\kappa^2\sin\beta) + b^2\kappa^2 - \rho^2}{1-\kappa^2} \\ &= \frac{-X_0^2(1-\kappa^2) + 2X_0(1-\kappa^2)X_0 + b^2\kappa^2 - \rho^2}{1-\kappa^2} \\ &= X_0^2 + \frac{b^2\kappa^2 - \rho^2}{1-\kappa^2}. \end{aligned} \tag{19}$$

The expression of X_0 and R as a function of the three model parameters α, κ, and h suffice to define the geometry of the GCS model. The construction of the conical legs is straightforward and the front part can easily be constructed with a computer program, which is given as a pseudo-code in the Appendix.

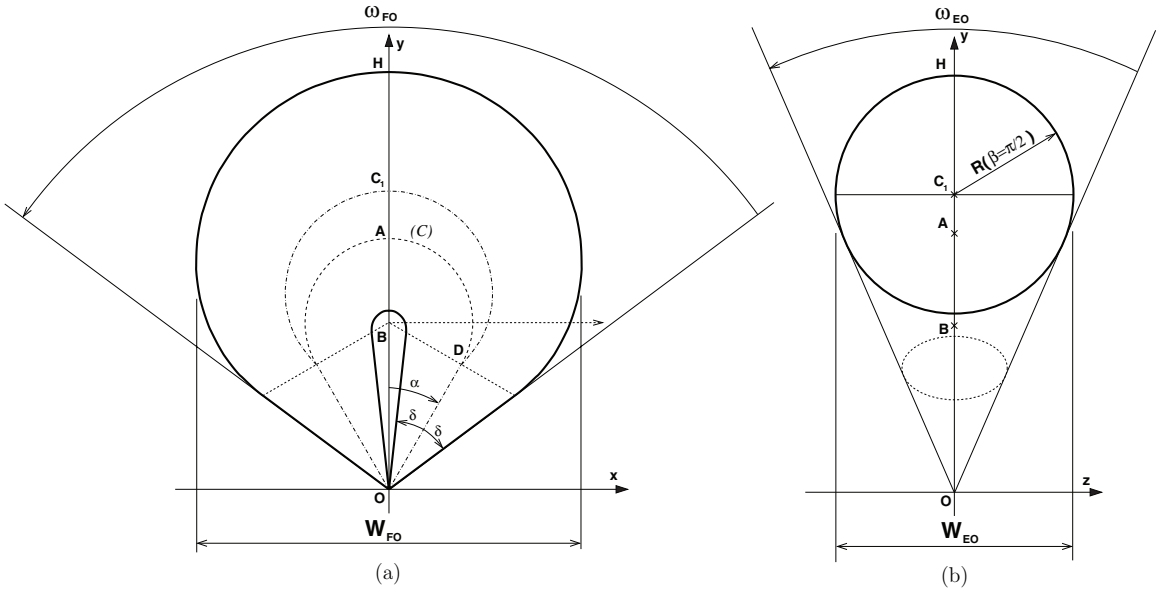

Figure 3. Schematic of the GCS model showing the dimensions given in Table 1.

2.3. Limiting Case: Ice-cream Cone when $\alpha \to 0$

We show here that the GCS model becomes equivalent to the well-known ice-cream cone model (Fisher & Munro 1984) when α tends toward 0. For example, this approach has been used by Patsourakos et al. (2010) to fit CMEs very close to the surface.

Setting $\alpha = 0$, then we have $\rho = 0$ and $b = h$ from Equations (6) and (4), and Equation (10) becomes

$$(x^2 + y^2 + z^2)(1 - \kappa^2) - 2yh + h^2 = 0. \quad (20)$$

If we translate the origin of the coordinate system of a distance y_0 along the y-axis,

$$y = y' + y_0, \quad (21)$$

then Equation (20) becomes

$$(x^2 + y'^2 + z^2)(1 - \kappa^2) - 2y'[h - y_0(1 - \kappa^2)] + h^2 - 2y_0h + y_0^2(1 - \kappa^2) = 0. \quad (22)$$

For this equation to be the equation of a sphere centered on the origin of this coordinate system, we need

$$y_0 = \frac{h}{1 - \kappa^2} \quad (23)$$

with the radius of the sphere being

$$R_s = \frac{h\kappa}{1 - \kappa^2}. \quad (24)$$

This way, we have shown that constraining Equation (20) to be a sphere when $\alpha = 0$ gives a non empty set of points that we call $\mathcal{S}_2$. But, since we have not used the same constraints as the more general case presented in Section 2.2, we need to show that $\mathcal{S}_2$ is equivalent to the set of points, $\mathcal{S}_1$, described by Equation (16) when $\alpha = 0$. For this purpose, we write the equation of the sphere $\mathcal{S}_2$ in the $(O, \boldsymbol{x}, \boldsymbol{y}, \boldsymbol{z})$ coordinate system:

$$x^2 + (y - y_0)^2 + z^2 = R_s^2, \quad (25)$$

and then we apply the same coordinate transforms as in Section 2.2. In $(O, \boldsymbol{X'}, \boldsymbol{Y}, \boldsymbol{z})$, the equation becomes

$$X'^2 + Y^2 + z^2 - 2X'[(y_0 - h)\sin\beta - X_0] - 2Y(y_0 - h)\cos\beta + h^2 + y_0^2 - 2hy_0 + X_0'^2 - 2X_0'(y_0 - h)\sin\beta = R_s^2. \quad (26)$$

As in Section 2.2, by constraining this equation to have the form of the equation of a circle of radius R' in the $Y = 0$ plane, we find $X_0' \equiv X_0(\alpha = 0)$ and $R' \equiv R(\alpha = 0)$ from Equations (18) and (19), respectively. Therefore, $\mathcal{S}_1 \equiv \mathcal{S}_2$, and the front part of the GCS model is spherical when the half-angle is zero.

2.4. Important Remark Concerning 2006 and 2009 Publication Notation

For the sake of simplicity in the publications of 2006 and 2009, the cross-section radius noted a is stated to be equal to κr, in Equation (1), with r the distance from the origin to a point of the shell. The parameter r is equivalent to OP in this present publication. Compared to Equation (7) in this present paper, a is not equal to the cross-section radius noted R, but it is equivalent to GP.

2.5. Formulae to Calculate Some of the Dimensions of the Model

The utility of the model is not restricted to the visual agreement with observations. One can derive several parameters that can be compared with physical measurements. Such parameters include, but are not restricted to, height of the leading edge, angular width, and shell cross-section radius.

The formulae are given in Table 1. Figure 3 shows the corresponding dimensions on the model schematic. Note that the face-on width, $W_{\rm FO}$, could not be expressed analytically, but it is possible to compute it numerically. The vector components of $\overrightarrow{BP}$ can be expressed as a function of β when P is bound to be in the $(O, \boldsymbol{x}, \boldsymbol{y})$ plane:

$$\overrightarrow{BP} = \overrightarrow{BC} + \overrightarrow{CP} = (X_0 + R)\begin{pmatrix}\cos\beta \\ \sin\beta \\ 0\end{pmatrix}, \quad (27)$$

Table 1
Formulae Giving Some of the GCS Model Dimensions

Description	Expression	
Heliocentric distance of the apex center	$OC_1 = b + X_0(\beta = \frac{\pi}{2}) = \frac{b+\rho}{1-\kappa^2}$	(28)
Cross-section radius of apex	$R(\beta = \frac{\pi}{2}) = \frac{\kappa(b+\rho)}{1-\kappa^2}$	(29)
Heliocentric height of the leading edge	$h_{\text{front}} = OH = \frac{b+\rho}{1-\kappa}$	(30)
Face-on angular width	$\omega_{\text{FO}} = 2(\alpha + \delta)$	(31)
Edge-on angular width	$\omega_{\text{EO}} = 2\delta$	(32)
Edge-on width	$W_{\text{EO}} = 2R(\beta = \frac{\pi}{2})$	(33)
Foot point separation on the surface of the sun	$d_{\text{FP}} = 2\alpha\, R_\odot$	(34)
Aspect ratio at apex	$\kappa = \frac{OC_1}{R(\beta=\pi/2)}$	(35)

with X_0 and R from Equations (18) and (19), respectively. Knowing that the half face-on width corresponds to the maximum of the x coordinate of $\overrightarrow{BP}$, W_{FO} can be estimated by finding the zero of the derivative of the x coordinate with respect to β.

3. CONCLUSION

In this paper, we have given the details of the GCS model derivation. The important aspects of the geometry are summarized here.

1. The GCS is constrained to expand in a self-similar way.
2. The front part is not circular, though it has been built using a circular generating line.
3. The cross section of the front part is a circle in the planes $(B, \overrightarrow{BG}, z)$.
4. The front of the GCS becomes spherical when the half-angle parameter is zero. In that case, it is equivalent to a hollow ice-cream cone.

We have also given different formulae for the calculation of various dimensions of the structure, as well as the pseudo-code for its implementation.

Most of the studies using the GCS have shown good agreement with CMEs observed in the *SOHO* LASCO C2-C3 (2.2–30 $R_\odot$) and *SECCHI* COR2 (3–20 $R_\odot$) fields of view. Patsourakos et al. (2010) used it in the EUVI field of view and found that by not restraining O to be at the center of the Sun, it allowed a better fitting of the events they studied. Above 30 $R_\odot$, observational evidences (Kahler & Webb 2007) as well as theoretical models (Riley & Crooker 2004) seem to show that the front of flux rope CMEs get distorted because of interactions with the ambient solar wind. The GCS model is not capable of reproducing such behavior, but we are considering ways to improve the model and account for this effect. This is one example of features that could be added to the model in future development.

I thank R. A. Howard for having the original idea of the GCS model. I also thank R. C. Colaninno for her careful reading and for checking the math, and A. Vourlidas and T. Nieves-Chinchil for their comments that greatly improved this manuscript. This work was supported by NASA.

APPENDIX

IMPLEMENTATION

The following pseudo-code gives the implementation of the GCS model. The input $\overrightarrow{OP} = (x, y, z)$ is a point in space where we want to evaluate the electron density. α, κ, h are the three parameters that define the geometry of the GCS model. Finally, σ_t, σ_l, and N_e are the parameters related to the electron density profile of the shell. As defined in Thernisien et al. (2006, 2009), we use a profile that is made of two half-Gaussian shaped functions:

$$N_e(d) = N_e \exp\left[-\left(\frac{R-d}{\sigma_s}\right)^2\right],$$
$$\text{with } \sigma_s = \begin{cases} \sigma_t, & \text{if } d < R, \\ \sigma_l, & \text{if } d \geqslant R \end{cases}. \tag{A1}$$

The pseudo-code is given here:

Require: $x, y, z, \alpha, \kappa, h, \sigma_t, \sigma_l, N_e$
if $y < 0$ **then**
return 0
end if
$b \leftarrow h/\cos\alpha$
$\rho \leftarrow h\tan\alpha$
testside $\leftarrow y + x\tan\alpha - b$
if testside < 0 **then**
{Leg side}
$\overrightarrow{OQ} \leftarrow$ orthoproj((0, 0, 0), (sin α, cos α, 0), (x, y, z))
$R \leftarrow \|\overrightarrow{OQ}\|\kappa/\sqrt{1-\kappa^2}$
$\|\overrightarrow{QP}\| \leftarrow \|\overrightarrow{OP} - \overrightarrow{OQ}\|$
if $(R - \|\overrightarrow{QP}\|) \geqslant 0$ **then**
$\sigma \leftarrow \sigma_t$
else
$\sigma \leftarrow \sigma_l$
end if
return $N_e \exp -\frac{(R-\|\overrightarrow{QP}\|)^2}{\sigma^2}$
else
{Front side}
$\beta \leftarrow$ atan2$(y - b, x)$
$X_0 \leftarrow (\rho + b\kappa^2\sin\beta)/(1-\kappa^2)$
$\overrightarrow{OC} \leftarrow (X_0\cos\beta, b + X_0\sin\beta, 0)$
$\|\overrightarrow{CP}\| \leftarrow \|\overrightarrow{OP} - \overrightarrow{OC}\|$
$R \leftarrow \sqrt{X_0^2 + (b^2\kappa^2 - \rho^2)/(1-\kappa^2)}$
if $(R - \|\overrightarrow{CP}\|) \geqslant 0$ **then**
$\sigma \leftarrow \sigma_t$
else
$\sigma \leftarrow \sigma_l$
end if
return $N_e \exp -\frac{(R-\|\overrightarrow{CP}\|)^2}{\sigma^2}$
end if

The function *orthoproj* calculates the projection of a point on a straight line. This is computed using this expression:

$$\overrightarrow{OQ} = \overrightarrow{OM} + \frac{1}{\vec{u}^2}[(\overrightarrow{OP} - \overrightarrow{OM}) \cdot \vec{u}]\vec{u}. \quad \text{(A2)}$$

The function takes three arguments: the first is a point of the straight line, noted M in Equation (A2). The second is a vector direction of that straight line, noted $\vec{u}$. The third argument is the point in space, noted P, we want to determine the projection on the straight line. The function returns the position of the projected point, noted Q.

An implementation of this code has been done in C++ and in IDL. The software, named *scraytrace*, is available in SolarSoft (Freeland & Handy 1998), under the *SECCHI* branch.

REFERENCES

Billings, D. E. 1966, A Guide to the Solar Corona (New York: Academic)
Brueckner, G. E., et al. 1995, Sol. Phys., 162, 357
Chen, J., Marqué, C., Vourlidas, A., Krall, J., & Schuck, P. W. 2006, ApJ, 649, 452
Chen, J., et al. 1997, ApJ, 490, L191
Chen, J., et al. 2000, ApJ, 533, 481
Cremades, H., & Bothmer, V. 2004, A&A, 422, 307
Domingo, V., Fleck, B., & Poland, A. I. 1995, Sol. Phys., 162, 1
Fisher, R. R., & Munro, R. H. 1984, ApJ, 280, 428
Freeland, S. L., & Handy, B. N. 1998, Sol. Phys., 182, 497
Howard, R. A., Sheeley, N. R., Jr., Michels, D. J., & Koomen, M. J. 1985, J. Geophys. Res., 90, 8173
Howard, R. A., et al. 2008, Space Sci. Rev., 136, 67
Kahler, S. W., & Webb, D. F. 2007, J. Geophys. Res. (Space Phys.), 112, A09103
Kaiser, M. L., Kucera, T. A., Davila, J. M., St. Cyr, O. C., Guhathakurta, M., & Christian, E. 2008, Space Sci. Rev., 136, 5
Liu, Y., Thernisien, A., Luhmann, J. G., Vourlidas, A., Davies, J. A., Lin, R. P., & Bale, S. D. 2010, ApJ, 722, 1762
Lynch, B. J., Li, Y., Thernisien, A. F. R., Robbrecht, E., Fisher, G. H., Luhmann, J. G., & Vourlidas, A. 2010, J. Geophys. Res. (Space Phys.), 115, A07106
Patsourakos, S., & Vourlidas, A. 2011, A&A, 525, A27
Patsourakos, S., Vourlidas, A., & Kliem, B. 2010, A&A, 522, A100
Poomvises, W., Zhang, J., & Olmedo, O. 2010, ApJ, 717, L159
Riley, P., & Crooker, N. U. 2004, ApJ, 600, 1035
Thernisien, A., Vourlidas, A., & Howard, R. A. 2009, Sol. Phys., 256, 111
Thernisien, A. F. R., Howard, R. A., & Vourlidas, A. 2006, ApJ, 652, 763